RESEARCH PAPER

Channels 5:3, 1-1; May/June 2011; © 2011 Landes Bioscience

Functional roles of $Ca_v1.3$, $Ca_v3.1$ and HCN channels in automaticity of mouse atrioventricular cells

Insights into the atrioventricular pacemaker mechanism

Laurine Marger,[1-3] Pietro Mesirca,[1-3] Jacqueline Alig,[4] Angelo Torrente,[1-3] Stefan Dubel,[1-3] Birgit Engeland,[4] Sandra Kanani,[1-3] Pierre Fontanaud,[1b-3] Jörg Striessnig,[5] Hee-Sup Shin,[6] Dirk Isbrandt,[4] Heimo Emke,[7] Joël Nargeot,[1-3] Matteo E. Mangoni[1-3,*]

[1]CNRS; UMR-5203; Institut de Génomique Fonctionnelle; Département de Physiologie; [1b]Département d'Endocrinologie; Montpellier, France; [2]INSERM; U661; Montpellier, France; [3]Universités de Montpellier 1and 2; UMR-5203; Montpellier, France; [4]Center for Obstetrics and Pediatrics; and Center for Molecular Neurobiology; RG Experimental Neuropediatrics; [7]Department of Vegetative Physiology and Pathophysiology; Center for Experimental Medicine; University Medical Center Hamburg-Eppendorf; Hamburg, Germany; [5]Department of Pharmacology and Toxicology; Institute of Pharmacy; Center for Molecular Biosciences; University of Innsbruck; Innsbruck, Austria; [6]Center for Neural Science; Korea Institute of Science and Technology; Cheongryang, Seoul, Republic of Korea

Key words: genetically-engineered mice, pacemaker activity, atrioventricular node, congenital heart block, sino-atrial node dysfunction, ion channels, $Ca_v1.3$ channels, $Ca_v3.1$ channels, HCN channels, electrophysiology, conduction, heart rate

Abberviations: AVN, atrioventricular node; SAN, sino-atrial node; $I_{Ca,L}$, L-type Ca^{2+} current; $I_{Ca,T}$, T-type Ca^{2+} current; I_f, hyperpolarization-activated f-current; $Ca_v1.3$, voltage-dependent L-type Ca^{2+} channel 3rd isoform; $Ca_v3.1$, voltage-dependent T-type Ca^{2+} channel 1st isoform; HCN, hyperpolarization-activated cation channel; CHB, congenital heart block; SNDD, sino-atrial dysfunction and deafness syndrome

The atrioventricular node controls cardiac impulse conduction and generates pacemaker activity in case of failure of the sino-atrial node. Understanding the mechanisms of atrioventricular automaticity is important for managing human pathologies of heart rate and conduction. However, the physiology of atrioventricular automaticity is still poorly understood. We have investigated the role of three key ion channel-mediated pacemaker mechanisms namely, $Ca_v1.3$, $Ca_v3.1$ and HCN channels in automaticity of atrioventricular node cells (AVNCs). We studied atrioventricular conduction and pacemaking of AVNCs in wild-type mice and mice lacking $Ca_v3.1$ ($Ca_v3.1^{-/-}$), $Ca_v1.3$ ($Ca_v1.3^{-/-}$), channels or both ($Ca_v1.3^{-/-}$/$Ca_v3.1^{-/-}$). The role of HCN channels in the modulation of atrioventricular cells pacemaking was studied by conditional expression of dominant-negative HCN4 channels lacking cAMP sensitivity. Inactivation of $Ca_v3.1$ channels impaired AVNCs pacemaker activity by favoring sporadic block of automaticity leading to cellular arrhythmia. Furthermore, $Ca_v3.1$ channels were critical for AVNCs to reach high pacemaking rates under isoproterenol. Unexpectedly, $Ca_v1.3$ channels were required for spontaneous automaticity, because $Ca_v1.3^{-/-}$ and $Ca_v1.3^{-/-}$/$Ca_v3.1^{-/-}$ AVNCs were completely silent under physiological conditions. Abolition of the cAMP sensitivity of HCN channels reduced automaticity under basal conditions, but maximal rates of AVNCs could be restored to that of control mice by isoproterenol. In conclusion, while $Ca_v1.3$ channels are required for automaticity, $Ca_v3.1$ channels are important for maximal pacing rates of mouse AVNCs. HCN channels are important for basal AVNCs automaticity but do not appear to be determinant for β-adrenergic regulation.

Supplementary Material

*Correspondence to: Matteo E. Mangoni; Email: matteo.mangoni@igf.cnrs.fr
Submitted: 02/18/11; Revised: 02/22/11; Accepted: 02/22/11
DOI:

Online Expanded Section

Supplemental Expanded Methods

Electrocardiogram (ECG) recording in conscious $Ca_v1.3^{-/-}$, $Ca_v3.1^{-/-}$ and $Ca_v1.3^{-/-}/Ca_v3.1^{-/-}$ mice.

For telemetric ECG recording, adult male mice were anesthetized with 2% isofluorane. A midline incision was made on the back along the spine to insert a telemetric transmitter (TA10EA-F20, Data Sciences International) into a subcutaneous pocket with paired wire electrodes placed over the thorax (chest bipolar ECG lead). Local anaesthesia was obtained with lidocaine (1%) injected subcutaneously at the sites of electrodes and transmitter implantation. To manage possible post-surgery pain, Advil (paracetamol and ibuprofene, 7mL/l) was added to the drinking water for four days after implantation). Experiments were initiated at least 8 days after recovery from surgical implantation. Mice were housed in individual cages with free access to food and water and were exposed to 12-hour light/dark cycles (light, 8:30 AM to 8:30 PM) in a thermostatically controlled room. ECG signals were recorded with the use of a telemetry receiver and an analog-to-digital conversion data acquisition system for display and analysis by Dataquest™ A.R.T.™ software (Data Sciences International). Heart rate and atrioventricular conduction (PR) values were determined from RR intervals. Mean heart rate values were obtained in each mouse for an overall 24-hour period from 8:30 AM to 8:30 PM and for the corresponding 12-hour light and dark periods. ECG parameters were measured with ECG Auto 1.5.7 software. Isolated P waves were counted in 30 s long stretches of recordings each 30 minutes for at least 3 hours and averaged.

Staining of AVNCs

Mouse AVNCs were isolated using the same protocol as used for patch clamping. AVNCs were placed into chambers and allowed to attach to Cell-Tak coated wells (3.5 μg/cm^2) for 1 hr (LAB-TEK II Chamber Slide, NUNC). Cells were then fixed with 4% paraformaldehyde for 20 minutes at room

temperature (RT), followed by soaking in 1xPBS for several hours. 250 µl of 2% Bovine Serum Albumin (Sigma) containing rat HCN4 monoclonal antibody (SHG 1E5, Santa Cruz, 1:100), anti mouse HA monoclonal (clone HA7, 1:250) were added and allowed to incubate overnight at 4 degrees in a humid chamber. The tissue was rinsed for 4 x 15 minutes (1x PBS). Goat anti-rat FITC secondary (Molecular Probes, 1:500), donkey anti mouse Alexa-647 (Molecular Probes,1:500), DAPI was incubated for 90 minutes at RT followed by 4 x 15 minutes (1xPBS). Prolong gold (Invitrogen) was overlayed and a glass coverslip gently placed over the sample. Images were taken with a Leica confocal microscope (Leica SPE) at the Montpellier RIO Imaging facility of the Arnaud de Villeneuve Campus (Montpellier, France). Image analysis was carried out on Metamorph Image Analysis software.

The specificity of Rat HCN4 antibody was confirmed using a mouse monoclonal HCN4 antibody (Neuromab), which had the identical overlapping staining pattern. Furthermore, SANCs expressing HCN4-HA tagged subunits showed overlapping staining using rat HCN4/mouse HA antibodies or mouse HCN4/rat HA antibodies (data not shown).

Isolation of mouse SANCs and AVNCs

Details on dissection of the mouse atrioventricular node can be found in the accompanying paper. [1] Beating hearts were removed under general anesthesia, consisting of 0.01 mg/g of Xylazine (Rompun 2%, Bayer AG, Leverkusen Germany), 0.1 mg/g of Ketamine (Imalgène, Merial, Bourgelat France) and 0.2 mg/g of Na-Pentobarbital (CEVA, France). The SAN and the AVN were exposed by using the landmarks shown in Fig. S1A,B and then excised in pre-warmed (35°C) Tyrode solution containing (mM/L): NaCl, 140; KCl, 5.4; $CaCl_2$, 1.8; $MgCl_2$, 1; Hepes-NaOH, 5; and D-glucose, 5.5; (adjusted to pH=7.4 with NaOH). SAN tissue strips were then transferred into a "low-Ca^{2+}-low-Mg^{2+}" solution containing (in mM/L): NaCl, 140; KCl, 5.4; $MgCl_2$, 0.5; $CaCl_2$, 0.2; KH_2PO_4, 1.2; taurine, 50; D-glucose, 5.5; bovine serum albumin (BSA), 1 mg/ml; Hepes-NaOH, 5; (adjusted to pH=6.9 with NaOH). SAN and AVN tissues were digested by adding collagenase type II or IV (229 U/ml, Worthington Biochemical Corporation, Lakewood, NJ, USA), elastase (1.9 U/ml, Worthington Biochemical Corporation, Lakewood, NJ, USA), protease (0.9 U/ml, Sigma, St. Quentin Fallavier, France), BSA 1mg/ml, and 200 µM $CaCl_2$. Digestion was

carried out for a variable time of 20-25 minutes at 35 °C. Tissue strips were then washed, and transferred into a modified "Kraftbrühe" (KB) medium [2] containing (in mM/L): L-glutamic acid, 70; KCl, 20; KOH, 80; (±)D-b-OH-butyric acid, 10; KH_2PO_4, 10; taurine, 10; BSA, 1mg/ml; and Hepes-KOH, 10; (adjusted to pH=7.4 with KOH). Single SAN and AVN cells were isolated by manual agitation in KB solution at 35 °C for 2-5 minutes.

Cellular automaticity was recovered by re-adapting the cells to a physiological extracellular Ca^{2+} concentration by addition of a solution containing (in mM/L): NaCl, 10, $CaCl_2$, 1.8, and normal Tyrode solution containing BSA (1mg/ml). The final storage solution contained (mM/L): NaCl, 100; KCl, 35; $CaCl_2$, 1.3; $MgCl_2$, 0.7; L-glutamic acid, 14; (±)D-b-OH-butyric acid, 2; KH_2PO_4; 2; taurine, 2; BSA 1mg/ml; (pH=7.4), and gentamycin (50 μg/ml). All chemicals were from Sigma (St Quentin, Fallavier), except for the (±)D-β-OH-butyric acid that was from Fluka Chemika (Buchs, CH), TTX and ZD 7288 that were from Tocris Bioscience (Ellisville, USA), 293B was a generous gift by Dr. Lang and E-4031 that was a generous gift by Dr. Flavien Charpentier (L' Institut du Thorax, Nantes).

Electrophysiological Recordings

For electrophysiological recordings, aliquots of the cell suspension were harvested in custom made recording chambers (working volume 500 μL) allowing unidirectional flow of solutions and mounted on the stage of an inverted microscope (Olympus, X71), and continuously perfused with normal Tyrode solution. The recording temperature was set to 36°C. The whole-cell variation of the patch-clamp technique [3] was used to record cellular ionic currents, by employing an Axopatch 200A (Axon Instruments Inc., Foster USA) patch-clamp amplifier, connected to the ground by an agar bridge filled with 150 mM KCl. Cellular automaticity was recorded by the perforated patch technique with escin (50 μM). Recording electrodes were fabricated from borosilicate glass, by employing a Flaming-Brown microelectrode puller (Sutter, Novato CA, USA). For recording cell automaticity, as well as I_f, we used an intracellular solution containing (mM/L): K^+-aspartate, 130; NaCl, 10; ATP-Na^+ salt, 2; creatine phosphate, 6.6; GTP-Mg^{2+}, 0.1; $CaCl_2$, 0.04 (pCa=7); Hepes-KOH, 10; (adjusted to pH=7.2 with KOH). Electrodes had a resistance of about 5 MΩ. Seal resistances were in the range of 2-5 GΩ.

For recording of calcium currents (I_{CaT}, $I_{Ca,L}$), we replaced K-Aspartate and KCl in the intracellular solution, with an equal amount of CsCl. The extracellular solution contained (in mM/L): tetraetylammonium-chloride (TEA-Cl), 130; $CaCl_2$, 2; $MgCl_2$, 1; 4-amino-pyridine, 10; Hepes, 25; (adjusted to pH=7.4 with TEAOH). I_{Kr} was recorded in Tyrode, after addition of 10 μM TTX, and 0.3 μM isradipine. I_f was routinely recorded in Tyrode solution containing 5 mM $BaCl_2$ to block I_{K1} [4]. We performed data acquisition by using the pClamp software (ver. 9, Axon Instruments Inc.).

Data Analysis

The AP parameters were calculated as reported previously [5-7]. The following action potential (AP) parameters were calculated: the AP duration (APD), the slopes of the diastolic depolarisation (SDD), the maximum diastolic potential (MDP), the AP threshold (E_{th}), the maximum upstroke velocity (the peak of the first derivative of the AP waveform dv/dt), and the AP amplitude (APA). The cell membrane capacitance has been monitored by applying brief (10 ms) voltage steps of ±10 mV amplitude from a holding potential (HP) of −35 mV. Cav-mediated Ca^{2+} currents and I_{Na} were analyzed as previously reported [7, 8].

We performed analysis by employing the Origin Lab software (ver. 7.5, Microcal Inc., Northampton MA, USA). Results are presented as means ± the standard error of the mean (S.E.M, number of cells). For calculating the level of significance, the Student's t-test, the one- or two-way ANOVA tests followed by Tukey's post-hoc test and non-parametric Kruskal-Wallis test have been employed. When testing statistical differences results were considered significant with $p<0.05$. In all figures (*) indicates $p<0.05$, (**) $p<0.01$ and (***) $p<0.001$, respectively.

Numerical modelling of AVNC automaticity

Numerical modeling of AVNCs pacemaker activity was performed as described previously.[8] The numerical model by Mangoni et al [8] simulating pacemaking of mouse SANCs was adapted to AVNCs. We introduced two modifications in the SANC model source code. First, HCN-mediated I_f current was modeled according to the allosteric model of f-channel dual gating by voltage and cAMP developed by DiFrancesco.[9] Second we included SK2-mediated Ca^{2+}-dependent K^+ current (I_{SK2}) recently described in mouse AVNCs [10] by setting its conductance as a function of $Ca_v1.3$-mediated $I_{Ca,L}$ density as reported in mouse atrial myocytes. [11] We found that adding I_{SK2} to the AVNC model better fitted the ratio between the diastolic interval and the action potential duration.

We then adapted model parameters according to densities and activation of ionic currents we recorded in native WT AVNCs. Results of this characterization of ionic currents in mouse AVNCs are shown in the accompanying paper "*Pacemaker activity and ionic currents in mouse atrioventricular node cells*". [1] We modified the original parameters list from Mangoni et al [8] SANC model according to the following Table. Abbreviations are the same as in SANC models by Zhang et al [12] and by Mangoni et al. [8] Numerical simulations were carried out using the JSim software available at: http://www.physiome.org/jsim/. The AVNCs model source code is freely available upon request.

Abbreviation	Absolute value	Abbreviation	Absolute value
C_m	21 pF	$I_{Na}\ V_{1/2act}$	-43 mV
d_{NaCa}	0.0001	$I_{Na}\ V_{1/2Inact}$	-65 mV
$E_{Ca,L}$	46.4 mV	G_{Nas} *(TTX sensitive)*	$3.4x10^{-6}$ µS
$E_{Ca,T}$	45 mV	$I_{Nas}\ V_{1/2act}$	-32 mV
G_{Nar} *(TTX resistant)*	$1.1x10^{-5}$ µS	$I_{Nas}\ V_{1/2Inact}$	-56 mV

$g_{Ca,L}$	0.0004 µS	k_{NaCa}	0.000027 nA
$I_{Ca,L}$ $V_{1/2act}$ ($Ca_v1.2$)	-3 mV	$[Na^+]_o$	140 mM
$I_{Ca,L}$ $V_{1/2Inact}$ ($Ca_v1.2$)	-28 mV	$[Na^+]_i$	8 mM
$g_{Ca,D}$	0.002 µS	$[Ca^{2+}]_o$	2 mM
$I_{Ca,D}$ $V_{1/2act}$ ($Ca_v1.3$)	-23 mV	$[Ca^{2+}]_i$	0.0001 mM
$I_{Ca,D}$ $V_{1/2Inact}$ ($Ca_v1.3$)	-48 mV	$[K^+]_o$	5.4 mM
$g_{Ca,T}$	0.0038 µS	$[K^+]_i$	140 mM
$I_{Ca,T}$ $V_{1/2act}$ ($Ca_v3.1$)	-45 mV	$[cAMP]_i$	0.003
$I_{Ca,T}$ $V_{1/2Inact}$ ($Ca_v3.1$)	-71 mV		
g_{st}	0.017 µS		
g_{K1}	0.0025 µS		
$g_{K,r}$	0.005 µS		
Pinac	-15		
$F_{K,r}$	0.4		
g_{to}	0.00049 µS		
g_{sus}	0.000065 µS		
g_{SK2} (with 0 $g_{Ca,D}$)	0.000518 µS		
$g_{f,Na}$	0.0024 µS		
$g_{f,K}$	0.0024 µS		
I_f ($V_{1/2act}$)	-101 mV		
$g_{b,Na}$	0.000058 µS		
$g_{b,Ca}$	0.0000152 µS		
$g_{b,K}$	0.0000252 µS		
I_{pmax}	0.0478 nA		
$K_{m,K}$	0.621		
$K_{m,Na}$	5.64		
γ_{NaCa}	0.5		

Supplemental Results and Discussion

SI. Numerical modeling of AVNC automaticity

We developed a numerical model of AVNC automaticity. The model is based on the one presented in Mangoni et al [8] to reproduce mouse SANC automaticity. This approach may constitute a starting point to compare SANC and AVNC automaticity based on transmembrane ion channel clock mechanisms of pacemaking.

When the SANC model by Mangoni et al [8] is modified according to paremeters listed in the supplemental online Methods section, the prototype AVNCs model generated a basal pacemaking rate, which was slower than the one generated by the SANC model (Fig. S2A,B). Calculated AVNC pacemaking displayed a more negative maximum diastolic potential and action potential threshold than that observed in AVNCs. When the AVNC parameters where changed to that of the SANC model of pacemaking (except for $I_{Na,r}$ and $I_{Na,s}$ that were kept constant), pacemaking accelerated, the slope of the diastolic depolarization increased and the maximum diastolic potential shifted positively (Fig. S2B). This calculation is reminiscent of what we observed when comparing pacemaking of AVNCs and SANCs (see Fig.2 in the accompanying paper).

In our numerical simulations, we have introduced the two I_{Na} components $I_{Na,r}$ and $I_{Na,s}$ based on our voltage-clamp experiments on AVNCs.[1] These two current components activated in the late phase of the diastolic depolarization, the action potential threshold and upstroke (Fig. S2A). To evaluate the dependence of our AVNC model of pacemaking from I_{Na}, we set both $I_{Na,r}$ and $I_{Na,s}$ to zero (Fig. S2C). Simulated pacemaker activity stopped (Fig. S2C). The action potential threshold was function of I_{Na} density. When $I_{Na,r}$ and $I_{Na,s}$ densities were switched to the SANCs value [8] the threshold shifted positively (not shown). In conclusion, the model suggests that, as a consequence of the robust expression of I_{Na} in AVNCs, the action potential threshold approached that of $I_{Na,r}$ activation threshold. $I_{Na,r}$ appears also as the predominant contributor of the action upstroke velocity.

The AVNC numerical model suggested that the $Ca_v1.3$-mediated $I_{Ca,L}$ is present during the diastolic depolarization as a relatively small inward current (Fig. S2A). $Ca_v1.3$-mediated $I_{Ca,L}$ density is comparable to that of other inward currents, notably $Ca_v3.1$-mediated $I_{Ca,T}$ and HCN-mediated I_f current (Fig. S2A). The relatively low (compared to SANCs) absolute expression of $Ca_v1.3$-mediated $I_{Ca,L}$ may also explain the dependence of AVNC firing from I_{Na}. Indeed, because I_{Na} inhibition slows, but does not abolish SANC pacemaking [13], we run simulations in which $Ca_v1.3$-mediated activation and density were switched to SANC values (supplemental Fig. S3). In this case, abolition of I_{Na} did not stop completely pacemaking that set to a slower rate, with a more positive maximum diastolic potential, action potential threshold and reduced action potential amplitude. In the absence of I_{Na}, numerical modeling suggests that the action potential upstroke phase may be carried by $Ca_v1.3$-mediated and $Ca_v1.2$-mediated $I_{Ca,L}$.

Numerical modeling of $Ca_v3.1$-mediated $I_{Ca,T}$ inactivation suggested that these channels can contribute to AVNCs pacemaking because of activation of $Ca_v3.1$-mediated $I_{Ca,T}$ in the diastolic depolarization range (Fig. S2A, S4A, S5A).

In spite of its weaker density, and a more negative activation, HCN-mediated I_f significantly contributed to AVNC pacemaking, because hHCN4-573X expressing AVNCs had strongly reduced basal automaticity (Fig. 7). We thus attempted to model basal pacemaking in AVNCs expressing hHCN4-573X channels by shifting I_f activation curve negatively of -20 mV and setting cAMP concentration to zero. Slowing of calculated AVNC pacemaking was observed in the model (Fig. S4B). To further verify modeling results, we performed numerical simulations of partial I_f inhibition by 3 μM ZD-7228 as in current-clamp experiments on native AVNCs (Fig. S4C). The AVNCs model predicted about 10% slowing of pacemaking. This suggestion was consistent with experiment on native AVNCs.[1] We did not test the effects of doses of ZD-7228 higher than 3 μM in native AVNCs, because of potential interfering effects on I_{Kr}. In our model of AVNCs, switching the I_f density and activation to corresponding values observed in SANCs increased the slope of the diastolic depolarization and increased pacemaker activity (supplemental Fig. S5B). Setting the

cAMP concentration to saturating levels (3 μM) also accelerated simulated AVNC pacemaking (Fig. S5C).

When characterizing functionally native mouse WT AVNCs we found higher expression of I_{Kr} in AVNCs than in SANCs. In our model of AVNCs, a decrease of I_{Kr} density from the experimental value recorded in AVNCs[1] to that reported by Clark et al. in SANCs [14] shifted positively the maximum diastolic potential and slightly accelerated the rate of diastolic depolarization (supplemental Fig. S5D).

In conclusion, our modeling work suggests that differences in the degree of expression and activation of $Ca_v1.3$, $Ca_v3.1$ and HCN channels may contribute to the slower pacemaking in AVNCs than in SANCs. Beside these channels, other mechanisms can underlie AVNCs pacemaking. Among them, RYR-dependent Ca^{2+} release in AVNCs will need to be investigated in the future by both functional and numerical modeling strategies. In particular, RYR-dependent Ca^{2+}release[15] can be a potential candidate in the β-adrenergic regulation of AVNCs pacemaking in normal and mutant mice.

Supplemental References

1. Marger L, Mesirca P, Alig J, Torrente A, Dubel S, Engeland B, et al. Pacemaker activity and ionic currents in mouse atrioventricular node cells.
2. Isenberg G, Klockner U. Calcium tolerant ventricular myocytes prepared by preincubation in a "KB medium". Pflugers Archiv 1982; 395:6-18.
3. Hamill OP, Marty A, Neher E, Sakmann B, Sigworth FJ. Improved patch-clamp techniques for high-resolution current recording from cells and cell-free membrane patches. Pflugers Archiv - 1981; 391:85-100.
4. DiFrancesco D, Ferroni A, Mazzanti M, Tromba C. Properties of the hyperpolarizing-activated current (if) in cells isolated from the rabbit sino-atrial node. J Physiol 1986; 377:61-88.
5. Honjo H, Boyett MR, Kodama I, Toyama J. Correlation between electrical activity and the size of rabbit sino-atrial node cells. J Physiol 1996; 496:795-808.
6. Rocchetti M, Malfatto G, Lombardi F, Zaza A. Role of the input/output relation of sinoatrial myocytes in cholinergic modulation of heart rate variability. J Cardiovasc Electrophysiol 2000; 11:522-30.
7. Mangoni ME, Couette B, Bourinet E, Platzer J, Reimer D, Striessnig J, et al. Functional role of L-type Cav1.3 Ca^{2+} channels in cardiac pacemaker activity. Proc Natl Acad Sci U S A 2003; 100:5543-8.
8. Mangoni ME, Traboulsie A, Leoni AL, Couette B, Marger L, Le Quang K, et al. Bradycardia and slowing of the atrioventricular conduction in mice lacking CaV3.1/alpha1G T-type calcium channels. Circ Res 2006; 98:1422-30.
9. DiFrancesco D. Dual allosteric modulation of pacemaker (f) channels by cAMP and voltage in rabbit SA node. J Physiol 1999; 515:367-76.
10. Zhang Q, Timofeyev V, Lu L, Li N, Singapuri A, Long MK, et al. Functional roles of a Ca2+-activated K^+ channel in atrioventricular nodes. Circ Res 2008; 102:465-71.
11. Lu L, Zhang Q, Timofeyev V, Zhang Z, Young JN, Shin HS, et al. Molecular coupling of a Ca2+-activated K+ channel to L-type Ca^{2+} channels via alpha-actinin2. Circ Res 2007; 100:112-20.
12. Zhang H, Holden AV, Kodama I, Honjo H, Lei M, Varghese T, et al. Mathematical models of action potentials in the periphery and center of the rabbit sinoatrial node. Am J Physiol Heart Circ Physiol 2000; 279:H397-421.
13. Lei M, Jones SA, Liu J, Lancaster MK, Fung SS, Dobrzynski H, et al. Requirement of neuronal- and cardiac-type sodium channels for murine sinoatrial node pacemaking. J Physiol 2004; 559:835-48.
14. Clark RB, Mangoni ME, Lueger A, Couette B, Nargeot J, Giles WR. A rapidly activating delayed rectifier K^+ current regulates pacemaker activity in adult mouse sinoatrial node cells. Am J Physiol Heart Circ Physiol 2004; 286:H1757-66.
15. Lakatta EG, Maltsev VA, Vinogradova TM. A coupled SYSTEM of intracellular Ca2+ clocks and surface membrane voltage clocks controls the timekeeping mechanism of the heart's pacemaker. Circ Res 2010; 106:659-73.

Supplemental Tables

Supplemental Table S1. ECG intervals of $Ca_v3.1^{-/-}$, $Ca_v1.3^{-/-}$ and $Ca_v1.3^{-/-}/Ca_v3.1^{-/-}$ mice.

	WT		**$Ca_v3.1^{-/-}$**		**$Ca_v1.3^{-/-}$**		**$Ca_v1.3^{-/-}$ $Ca_v3.1^{-/-}$**		**p**	**p**	**p**	**p**	**p**	**p**
	A	**n**	**B**	**n**	**C**	**n**	**D**	**n**	**A*vs*B**	**A*vs*C**	**A*vs*D**	**B*vs*C**	**B*vs*D**	**C*vs*D**
RR (ms)	108 ± 4	9	129 ± 6	4	217 ± 15	8	224 ± 16	6	*	***	***	**	**	ns
PR (ms)	36 ± 1	9	40 ± 1	4	56 ± 1	8	66 ± 4	6	*	***	***	***	***	**
QRS (ms)	9 ± 0	9	9 ± 0	4	10 ± 0	8	9 ± 0	6	ns	ns	ns	ns	ns	ns
QT (ms)	46 ± 1	9	49 ± 1	4	55 ± 2	8	55 ± 4	6	ns	ns	ns	ns	ns	ns
QTc (ms)	44 ± 1	9	44 ± 1	4	38 ± 1	8	41 ± 4	6	ns	ns	ns	ns	ns	ns
2 PP	0	9	0	4	1.3 ± 0.6	8	5 ± 2	6	ns	*	**	ns	*	ns
3 PP	0	9	0	4	0.3 ± 0.3	8	2 ± 1	6	ns	ns	*	ns	*	ns

* $p<0.05$; ** $p<0.01$; ***$p<0.001$

Supplemental Table S2. Action potential parameters of mouse Wild-type (WT), $Ca_v3.1^{-/-}$, $Ca_v1.3^{-/-}$ and $Ca_v1.3^{-/-}/Ca_v3.1^{-/-}$ AVNCs. Abbreviations used are the same as in supplemental Table S2.

	WT		**$Ca_v3.1^{-/-}$**		**$Ca_v1.3^{-/-}$**		**$Ca_v1.3^{-/-}$ $Ca_v3.1^{-/-}$**		**p**	**p**	**p**	**p**	**p**	**p**
	A	**n**	**B**	**n**	**C**	**n**	**D**	**n**	**A vs B**	**A vs C**	**A vs D**	**B vs C**	**B vs D**	**C vs D**
Rate (bpm)	173 ± 27	8	52 ± 8	7	53 ± 8	7	24 ± 4	6	***	***	***	ns	*	*
MDP (mV)	-57 ± 1	8	-59 ± 2	7	-60 ± 2	7	-65 ± 2	6	ns	ns	*	ns	ns	ns
Eth (mV)	-41 ± 2	8	-44 ± 3	7	-44 ± 2	7	-47 ± 3	6	ns	ns	ns	ns	ns	ns
SDD (mV/ms)	0.05 ±0.01	8	0.016 ±0.005	7	0.007± 0.002	7	0.009 ±0.004	6	**	***	**	ns	ns	ns
APA (mV)	91 ±7	8	74 ± 5	7	70 ± 5	7	88 ± 4	6	ns	*	ns	ns	ns	ns
dV/dt (mV/ms)	13 ± 3	8	8 ± 3	7	9 ± 2	7	14 ± 3	6	ns	ns	ns	ns	ns	ns
APD (ms)	152 ± 18	8	270 ± 45	7	236 ± 38	7	305 ± 27	6	ns	ns	*	ns	ns	ns

* $p<0.05$; ** $p<0.01$; ***$p<0.001$

Supplemental Table S3. Action potential parameters of mouse Wild-type (WT), $Ca_v3.1^{-/-}$ and $Ca_v1.3^{-/-}$ AVNCs in control conditions and after perfusion of 0.1 μM ISO. Abbreviations used are the same as in supplemental Table S2.

		WT		$Ca_v3.1^{-/-}$		$Ca_v1.3^{-/-}$		p	p	p		p	
		A	n	C	n	B	n	A vs B	A vs C	B vs C		D vs E	
D	Rate (bpm)	173 ± 27	8	64 ± 6	5	54 ± 9	6	**	**	ns	* A	* B	** C
	MDP (mV)	-57 ± 1	8	-60 ± 3	5	-59 ± 3	6	ns	ns	ns	* A	ns B	ns C
	Eth (mV)	-41 ± 2	8	-43 ± 5	5	-43 ± 2	6	ns	ns	ns	ns A	ns B	* C
	SDD (mV/ms)	0.05 ± 0.01	8	0.021 ± 0.005	5	0.008± 0.002	6	**	***	ns	** A	* B	ns C
	APA (mV)	91 ±7	8	77 ± 8	5	70 ± 5	6	ns	*	ns	ns A	ns B	* C
	dV/dt (mV/ms)	13 ± 3	8	8 ± 4	5	9 ± 2	6	ns	ns	ns	ns A	ns B	ns C
	APD (ms)	152 ± 18	8	216 ± 54	5	217 ± 38	6	ns	ns	ns	ns A	ns B	ns C
E	Rate, ISO	222 ± 24	8	97 ± 11	5	78 ± 11	6	**	***	ns			
	MDP, ISO	-62 ± 1	8	-55 ± 1	5	-63 ± 1	6	**	ns	**			
	Eth, ISO	-44 ± 1	8	-37 ± 3	5	-47 ± 1	6	ns	ns	*			
	SDD, ISO	0.09±0.01	8	0.049 ± 0.03	5	0.020± 0.006	6	***	***	ns			
	APA, ISO	100 ±9	8	59 ± 6	5	84 ± 7	6	*	ns	ns			
	dV/dt, ISO	18 ± 4	8	2 ± 0.4	5	16 ± 5	6	ns	ns	ns			
	APD, ISO	150 ± 25	8	181 ± 36	5	211 ± 30	6	ns	*	**			

* $p<0.05$; ** $p<0.01$; ***$p<0.001$

Supplemental Table S4. Action potential parameters of control mono-transgenic (WTTG) and double-transgenic (TGTG) AVNCs expressing hHCN4-573X channels in control conditions and after perfusion of 0.1 μM ISO. Abbreviations used are the same as in supplemental Table S2.

		WTTG		TGTG		p	p	
		A	n	B	n	A vs B	C vs D	
	Cm (pF)	-23 ± 3	11	-31 ± 2	21	*		
C	If density$_{-120mV}$ (pA/pF)	-12 ± 2	6	-12 ± 3	9	ns	A **	B ns
	MDP (mV)	-59 ± 2	7	-50 ± 2	8	*	A ns	B ***
	Eth (mV)	-42 ± 2	7	-39 ± 3	8	ns	A ns	B ns
	SDD (mV/ms)	0.08 ± 0.02	7	0.03 ± 0.1	8	*	A *	B *
	APA (mV)	92 ± 11	7	60 ± 7	8	*	A ns	B *
	dV/dt (mV/ms)	14 ± 5	7	5 ± 3	8	ns	A ns	B ns
	APD (ms)	127 ± 14	7	134 ± 22	8	ns	A ns	B ns
D	If density$_{-120mV}$	-32 ± 7	6	-11 ± 3	9	*		
	MDP, ISO	-56 ± 2	5	-60 ± 2	7	ns		
	Eth, ISO	-41 ± 2	5	-43 ± 3	7	ns		
	SDD, ISO	0.12 ± 0.02	5	0.11 ± 0.2	7	ns		
	APA, ISO	97 ± 12	5	79 ± 9	7	ns		
	dV/dt, ISO	16 ± 5	5	7 ± 3	7	ns		
	APD, ISO	125 ± 11	5	167 ± 51	7	ns		

* $p<0.05$; ** $p<0.01$; ***$p<0.001$

Supplemental Figure Legends

Supplemental Fig S1. Numerical simulations of ionic currents in mouse AVNCs activated by voltage-clamp steps at potentials indicated by the colour code. Ca_v-mediated currents are shown in the upper row of the figure as indicated. The middle row shows simulated I_{Na} and I_{Kr} in mouse AVNCs. The bottom row shows calculated I_f in control conditions and under a saturating intracellular cAMP concentration. The shift of current activation is particularly evident at voltages between -100 and -70 mV.

Supplemental Fig S2. (A). Numerical simulation of AVNC automaticity showing the time course of I_{Na}, $Ca_v1.3$-mediated $I_{Ca,L}$, $Ca_v3.1$-mediated $I_{Ca,T}$ and HCN-mediated I_f during pacemaker activity. (B). Comparative simulation of AVNCs and SANCs pacemaking. Suppression of I_{Na} (C) or $Ca_v1.3$-mediated I_{CaL} blocks AVNC pacemaking (D).

Supplemental Fig S3.

This panel shows that when $Ca_v1.3$-mediated $I_{Ca,L}$ activation and half-activation voltage are switched to values corresponding to that recorded in SANCs, AVNC pacemaking no longer depends from I_{Na}. Pacemaking persists at a moderately slower rate than recorded when I_{Na} is present. In these conditions, $Ca_v1.3$-mediated $I_{Ca,L}$ drives most of the action potential upstroke phase.

Supplemental Fig S4.

(A). Abolition ($I_{Cav3.1}=0$) of $Ca_v3.1$-mediated $I_{Ca,T}$ induces slowing of AVNCs pacemaker activity.(C). Acceleration of pacemaking is calculated in AVNCs when $Ca_v3.1$-mediated $I_{Ca,T}$ density is switched to that recorded in SANCs. (B). In this numerical simulation of AVNC pacemaking, the cAMP concentration "seen" by HCN-mediated f-channels has been set to zero. In this condition, the

activation kinetics of f-channels becomes slower and I_f half-activation voltage shifts in the negative direction. This simulation recapitulates expression of cAMP-dependent regulation deficient hHCN4-573X channels in AVNC plasma membranes ($I_{HCN4573X}$). (C). Moderate (10%) slowing of AVNC pacemaking was observed when I_f conductance was inhibited by 34% (I_{fZD}) as in experiments with ZD-7228. [1]

Supplemental online Fig S4.

(A). Switching the density of $Ca_v3.1$-mediated $I_{Ca,T}$ to the value observed in SANCs significantly increased the slope of the diastolic depolarization and pacemaker activity of AVNCs. (B). An effect qualitatively similar to that in (A) is observed when I_f activation and density were switched to the values recorded in SANCs. The slope of the diastolic depolarization is specifically increased and AVNCs pacemaking accelerated. (C). Setting cAMP concentrations to saturating levels (3 μM) shifts I_f activation to more positive voltages and accelerates AVNCs pacemaking. (D). The higher expression of I_{Kr} may contribute to the more negative maximum diastolic potential observed in AVNCs than in SANCs. Indeed, when I_{Kr} density is switched to the SAN value the maximum diastolic potential is shifted positively.

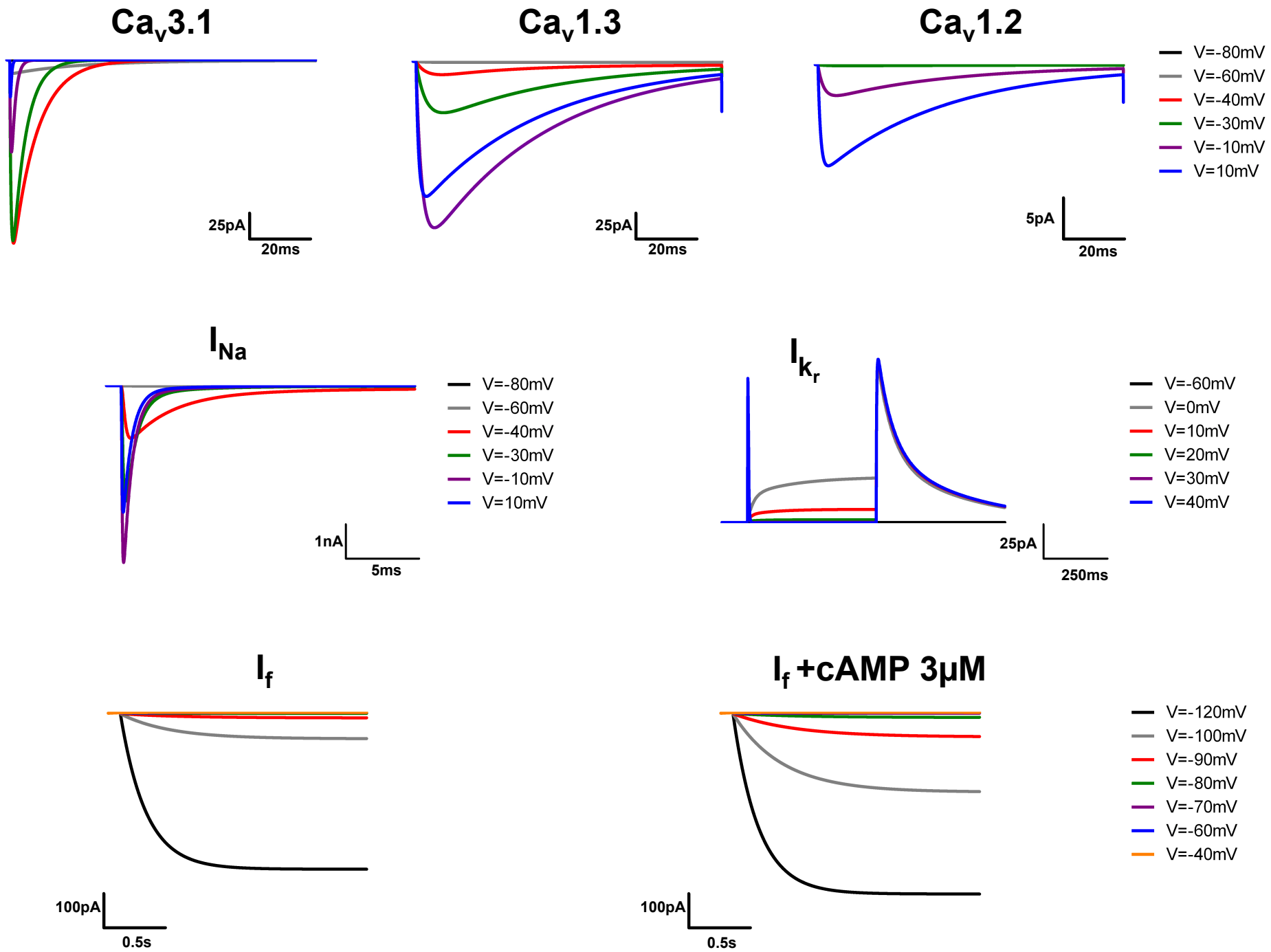
$Ca_v3.1$
$Ca_v1.3$
$Ca_v1.2$
V=-80mV
V=-60mV
V=-40mV
V=-30mV
V=-10mV
V=10mV
25pA
20ms
25pA
20ms
5pA
20ms
I_{Na}
V=-80mV
V=-60mV
V=-40mV
V=-30mV
V=-10mV
V=10mV
1nA
5ms
I_{k_r}
V=-60mV
V=0mV
V=10mV
V=20mV
V=30mV
V=40mV
25pA
250ms
I_f
100pA
0.5s
I_f +cAMP 3µM
V=-120mV
V=-100mV
V=-90mV
V=-80mV
V=-70mV
V=-60mV
V=-40mV
100pA
0.5s

Fig. S1

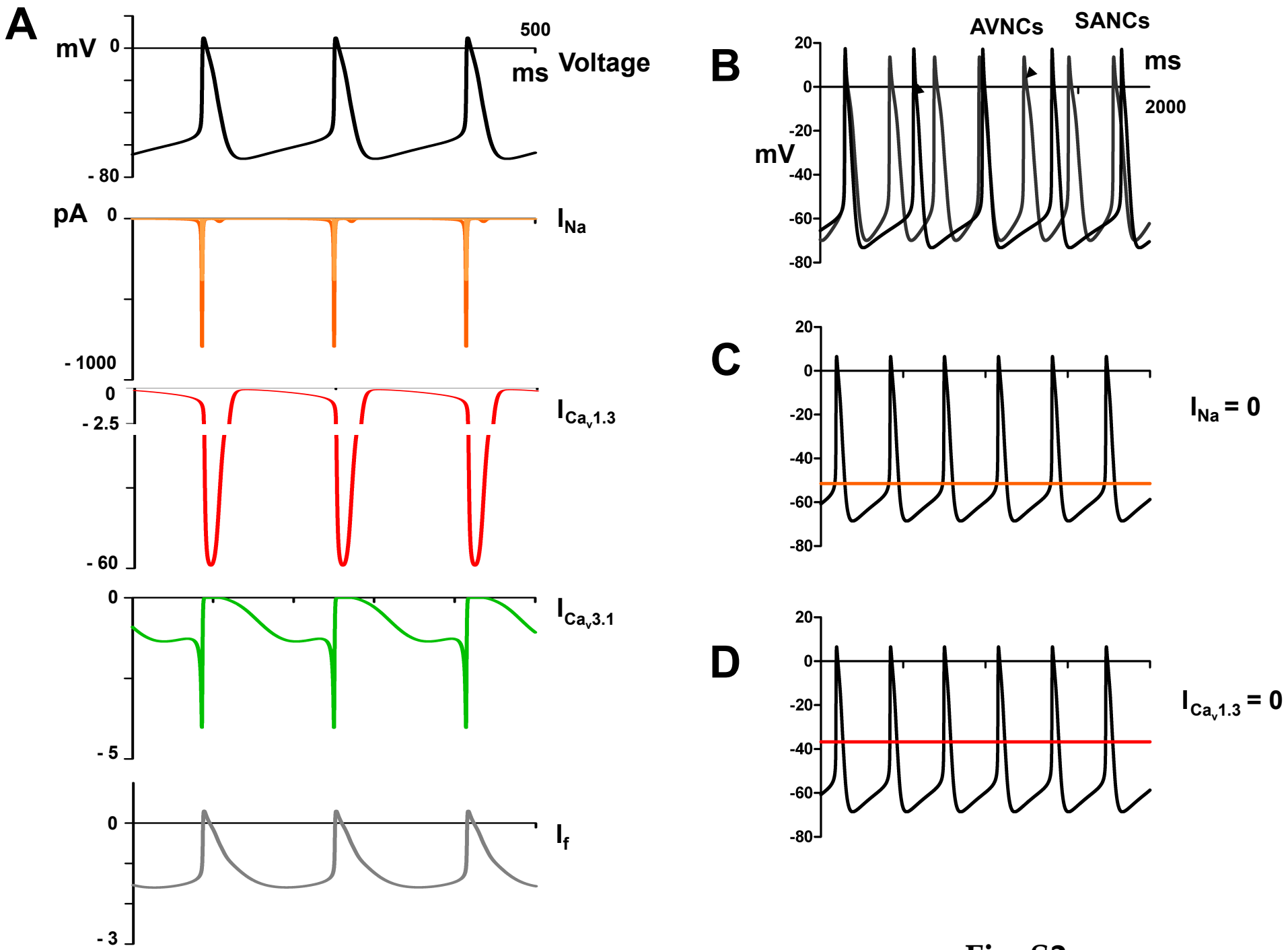
A
mV
0
500
ms
Voltage
- 80
pA
0
I_{Na}
- 1000
0
- 2.5
$I_{Ca_v1.3}$
- 60
0
$I_{Ca_v3.1}$
- 5
0
I_f
- 3
B
AVNCs
SANCs
20
0
-20
-40
-60
-80
mV
ms
2000
C
I_{Na} = 0
D
$I_{Ca_v1.3}$ = 0

Fig. S2

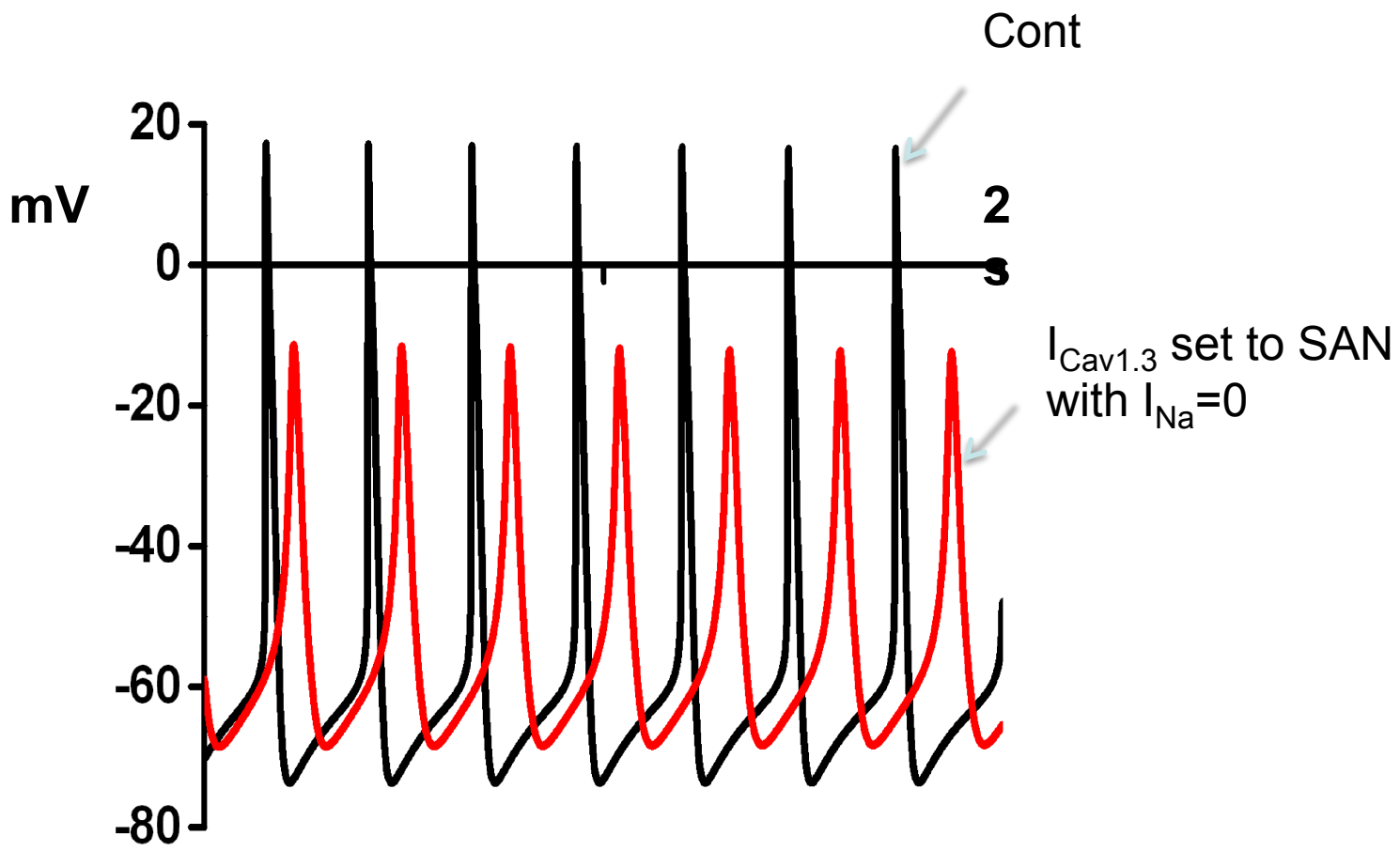

Fig. S3

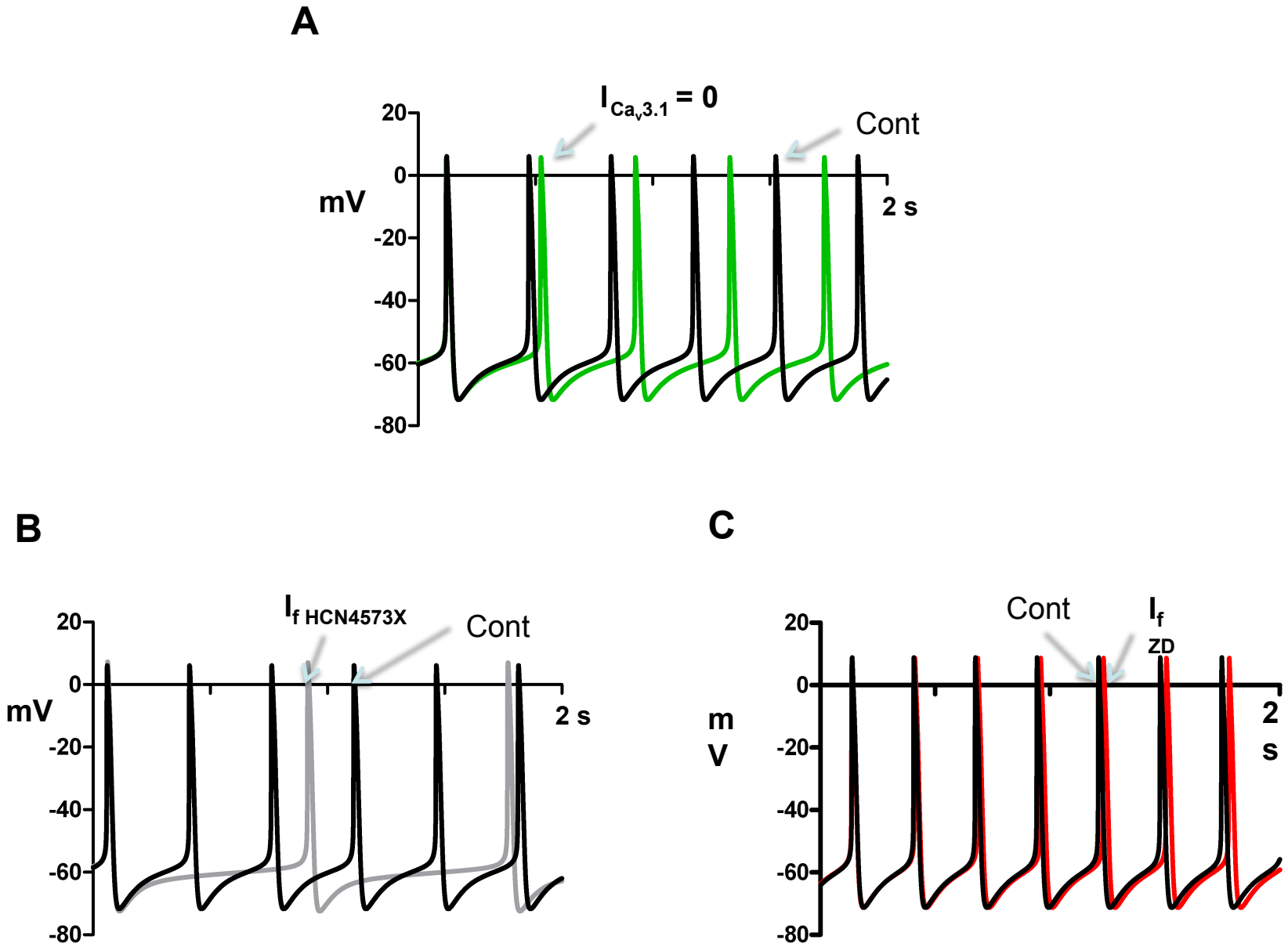
A
$I_{Ca_v3.1}$ = 0
Cont
20
0
-20
-40
-60
-80
mV
2 s
B
$I_{f\ HCN4573X}$
Cont
20
0
-20
-40
-60
-80
mV
2 s
C
Cont
I_f
ZD
20
0
-20
-40
-60
-80
m
V
2
s

Fig. S4

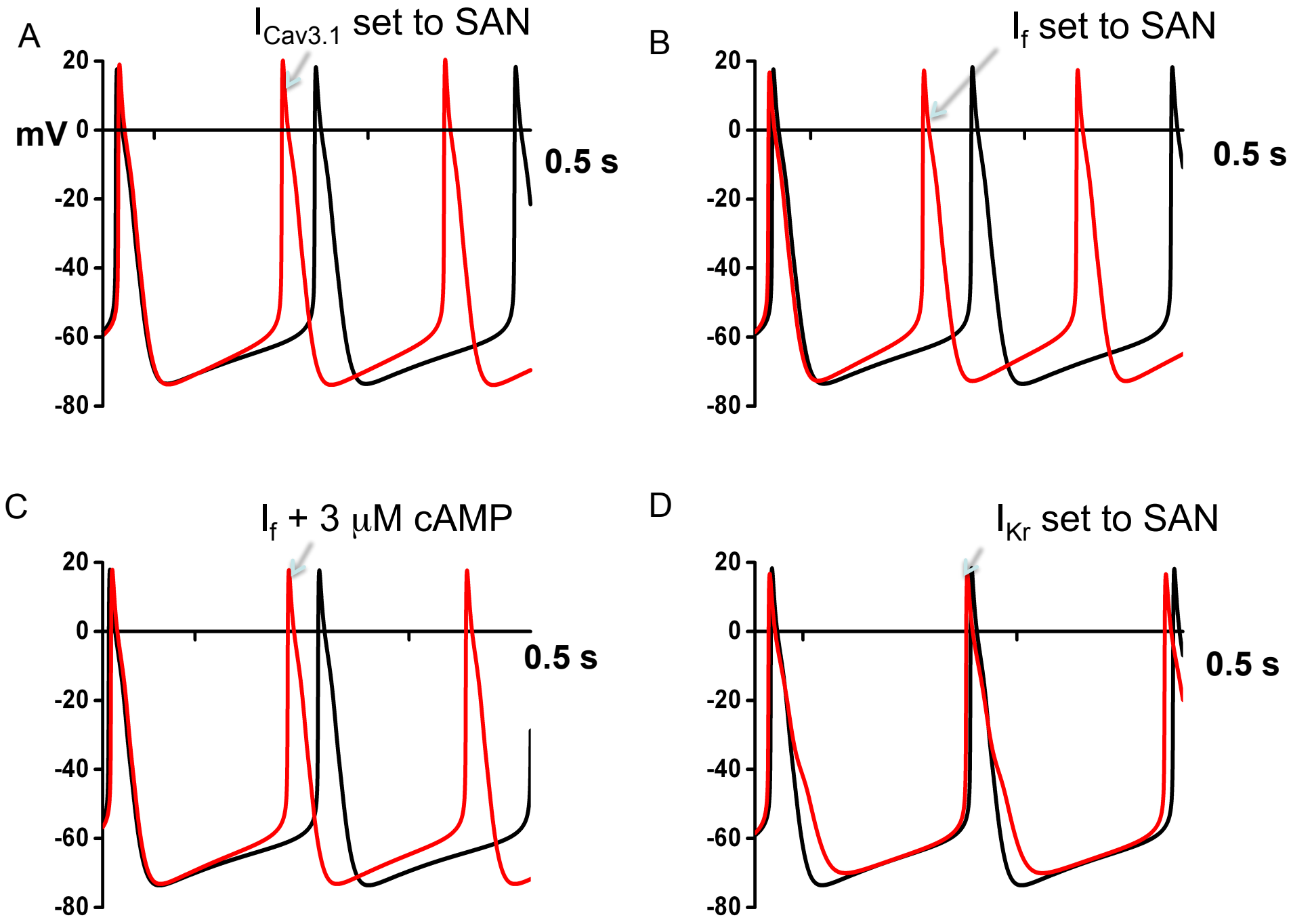
A
$I_{Cav3.1}$ set to SAN
mV
20
0
-20
-40
-60
-80
0.5 s
B
I_f set to SAN
20
0
-20
-40
-60
-80
0.5 s
C
I_f + 3 μM cAMP
20
0
-20
-40
-60
-80
0.5 s
D
I_{Kr} set to SAN
20
0
-20
-40
-60
-80
0.5 s

Fig. S5